UNIVERSITÀ DEGLI STUDI DI BERGAMO
Dipartimento di Ingegneria e Scienze applicate

Highlights

Manuscript name: "Experimental Investigation of the interaction between showerhead coolant jets and main flow"

- Measurement of adiabatic film cooling effectiveness in a vane showerhead by PSP
- Measurement of 3D flow field by PIV in the stagnation region
- Stagnation line moves towards the suction side due to coolant injection
- Jet separation and strong jet to mainstream interaction in the stagnation region
- High turbulence levels and high anisotropy especially along the span

24044 Dalmine (BG), viale Marconi 5 tel. 035 2052 327/334 fax 035 2052 077 e-mail: ingegneria@unibg.it
Università degli Studi di Bergamo www.unibg.it Cod. Fiscale 80004350163 P.IVA 01612800167

Experimental Investigation of the interaction between showerhead coolant jets and main flow

Giovanna Barigozzi[1*], Luca Casarsa[2], Fabio Pagnacco[2], Samaneh Rouina[1]

[1] Dipartimento di Ingegneria e Scienze Applicate - Università di Bergamo

Viale Marconi 5, 24044 Dalmine (BG) Italy

[2] Dipartimento di Ingegneria Elettrica, Gestionale e Meccanica - Università di Udine

Via delle Scienze 208, 33100 Udine Italy

Abstract

This paper presents the results of an experimental investigation into the thermal and aerodynamic behavior of coolant ejection at the leading edge of a highly loaded nozzle vane cascade. The leading-edge cooling scheme features four rows of cylindrical holes in a staggered configuration (showerhead). Pressure Sensitive Paints (PSP) technique was used to get the adiabatic film cooling effectiveness distribution, while Particle Image Velocimetry (PIV) and flow visualizations were used to investigate the mixing process taking place between coolant and main flow. PSP tests were conducted by using N_2 (Density Ratio DR=1.0) as coolant at variable blowing ratio (BR=2.0 – 4.0). Further tests were run by using CO_2 (DR=1.5) at matching BR and momentum flux ratio (I) in order to investigate the effects of density ratio. The BR = 3.0 injection case was selected for the PIV investigation. Thermal and flow field data consistently show a shift in the position of stagnation line towards the suction side. Jet liftoff close to stagnation and a strong jet to jet as well as jet to mainstream interaction were also observed, resulting in a complex 3D flow characterized by high turbulence levels with a high degree of anisotropy. No coherent structures were detected, supporting the random nature of mixing process.

Keywords: Gas turbine, Film cooling, Showerhead, PIV, PSP

1. INTRODUCTION

Cooling of high-pressure nozzle vanes, rotor blades and platform is mandatory in advanced gas turbines, whatever their application is: industrial, mechanical drive or propulsion. Advanced materials, thermal barrier coatings, and cooling techniques all contribute to reaching nowadays turbine inlet temperature (TIT) of the order of 1500°C, also meeting lifetime requirements. The high-pressure first nozzle vane cascade, being exposed to the hot gas coming from the combustor, experiences the highest thermal load. In particular, the leading edge region requires a very effective cooling system to sustain such a high-temperature level. The common approach to the protection of this critical region is to incorporate a dense array of discrete film cooling holes, typically referred as the showerhead. It generally consists of six to eight rows of coolant holes aligned normally to the mainstream and inclined in the span wise direction. This span wise inclination varies from manufacturer to manufacturer, but typically ranges between 25° and 50°. Moreover, holes lying on the vane hub side generally inject towards the tip while holes lying on the vane tip side inject towards the hub, making a symmetrical flow condition on the vane mid span section.

Most of the studies reported in the open literature focuses on the thermal aspect of showerhead film cooling through the measurement of adiabatic film cooling effectiveness and heat transfer coefficient. Over the past 30 years a vast number of studies investigated vane leading edge cooling on simplified models by considering different hole configurations under various operating conditions [1-6]. Wadia et al. [1] tested a leading edge full-coverage film cooled cylinder model with different hole spanwise inclination angles over a wide range of inlet Mach number conditions. The effectiveness levels were found to be dependent on the freestream Mach number as well as on the hole inclination angle. Other studies [2, 3] investigated the effect of hole shape on showerhead film cooling, showing that laid back shaped holes enhance the overall cooling performance of the showerhead system, compared to cylindrical holes. The influence of high mainstream turbulence on leading edge film cooling effectiveness and heat transfer coefficient was also investigated [4-6] in different blowing conditions. High turbulence levels were found to decrease the adiabatic effectiveness at low blowing ratios, but had little effect at high blowing ratios. Polanka et al. [7], and Witteveld et al. [8] measured film cooling effectiveness in the showerhead region of a simulated vane for low and high mainstream turbulence levels making use of infrared (IR) thermography and increasing the blowing ratio up to BR=2.9. This study revealed that the adiabatic film cooling effectiveness increased monotonically with increasing the blowing ratio due to the interaction of the coolant jets from laterally adjacent holes. However, this increase in the adiabatic effectiveness had been adversely affected by high mainstream turbulence [9]. Nathan et al. [10] also measured adiabatic film cooling effectiveness in the showerhead region of a model of a C3X turbine vane by increasing the momentum flux ratio up to I = 6.7. Their results were consistent with [7] and [8]. The most significant differences between film cooling performance at different blowing ratios are just in the front region of the leading edge [11].

Much less studies reporting measurements of the velocity field are available. Such information is important to get a better insight into the physical mechanisms associated with coolant jet to mainstream interaction as well as a reliable database to validate URANS, DES or LES CFD simulations. Recent studies revealed that coolant in the showerhead region does not stay attached to the surface, even at relatively low blowing ratios [12]. As the blowing ratio is increased, the coolant jet becomes more and more dissociated from the surface. This is theoretically explained by the lack of a cross flow along the stagnation line and by the deceleration of the main flow as it comes close to the surface [13]. Furthermore, LDV measurements [9] showed that not only build-up of coolant along the span of the airfoil makes CFD prediction of leading-edge difficult, due to the necessity for larger computational domain, but also mainstream interaction with cooling jets leads to extremely high turbulence levels, especially in the span wise component of turbulent fluctuations, which further complicates CFD simulations. Finally, showerhead cooling was also shown to modify the position of the approaching stagnation line [9, 14].

Numerous studies have assessed various RANS turbulence models' capabilities for predicting η and h compared to experimental data [15-19]. York et al. [15, 16] found that computational predictions for the laterally averaged effectiveness and the heat transfer ratio are in good agreement with experimental results, while Ledezma et al. [17] simulations either over or under-predicted the adiabatic effectiveness depending on the distance from the hole. Moreover, Heidmann et al. [18] performed steady simulations using k–ω turbulence model, yet results were not validated against measurements. Later, Dyson et al. [19] studies showed that SST k–ω turbulence model either over or under-predicted the adiabatic effectiveness depending on the BR value. Few numerical studies have considered the aerothermal behavior of the showerhead configuration compared to experimental measurements. Barigozzi and Ravelli [20] have shown that RANS prediction for the vane load, wake losses, and the plenum to mainstream pressure ratio matches quite well with experimental data, while a lack in the prediction capability of film cooling effectiveness distribution was observed, especially along the suction side.

In recent years, some studies took into account the unsteadiness to improve showerhead film cooling prediction by performing LES simulation considering only thermal measurement data [21-23]. Rozati et al. [21-22] results indicate the presence of an asymmetric counter-rotating vortex pair in the immediate wake of the coolant jet. However, this finding was not validated against experimental results. In addition, span-wise averaged adiabatic effectiveness and Frossling number were in good agreement with experimental data. Another study showed that DES predicted very well the spanwise-averaged effectiveness on the leading edge surface, yet some discrepancies in the local peak of effectiveness were observed [23].

The present paper contributes to the existing body of literature in documenting the interaction of showerhead coolant ejection with the main flow with both surface and off-wall measurements. Up to now, at author's knowledge, only few experimental data are available in the open literature as support to URANS, DES or LES results. The same cascade geometry and cooling configuration has been previously tested both experimentally (with the wide banded Thermo-Chromic Liquid Cristal technique) and numerically [24]. In this paper Particle Image Velocimetry (PIV) is used to investigate the unsteady mixing process taking place between coolant and main flow in the stagnation region. PSP technique is used to obtain the adiabatic film cooling effectiveness on the vane leading edge for variable BR in the range 2.0 to 4.0. As PIV tests could only be run injecting air as coolant, i.e. with a density ratio DR = 1, PSP results at variable DR are also presented to assess the influence of this parameter on showerhead film cooling in order to figure out the best scaling parameter with real engine condition. Moreover, PIV tests were run at a selected injection case of BR = 3.0 looking to the coolant to mainstream interaction both in the mid span blade to blade plane and along the vane span. This BR value of 3.0 was selected because it gives the best tradeoff between thermal protection in the leading edge region and coolant consumption. It also represents a challenging case for CFD simulation where jet lift off phenomena are relevant.

2. EXPERIMENTAL DETAILS

2.1 The model and the testing conditions

Tests were performed at the Energy Systems and Turbomachinery Laboratory of Bergamo University in cooperation with Udine University research team. The model consists in a 6 vane cascade whose central vane presents the showerhead cooling system depicted in Fig. 1. Airfoil geometry reported in Fig. 2 is typical of a high pressure nozzle vane of an industrial gas turbine. The model is characterized by a pitch to chord ratio of 1.04, an aspect ratio of 0.69, and the vane height H is 98 mm. The showerhead cooling scheme features four rows of cylindrical holes in a staggered configuration. This cooling configuration has to be considered just a portion of a more complex full coverage film cooling scheme for the whole vane; more specifically this hole layout is intended to cool the close vicinity of stagnation. Hole diameter (D) is 1 mm, hole length over diameter ratio L/D is 4.1. Holes are injecting coolant towards the vane tip with an injection angle of 45° in the span wise direction. Injection angle along the stream wise direction is 90°. Each row is composed of 16 cooling holes. Within each row hole to hole pitch is 5.88D, with cooling holes covering the 90% of the span. Row spacing is 5.1D in the stream wise direction: stagnation is expected to take place in between the holes, i.e. between row#2 and row#3. The cooled vane is made out of Plexiglas, assuring smooth surfaces. Coolant air was conveyed by a 3kW radial fan to a plenum chamber, connected to the vane by a flexible duct. A second plenum was realized inside of the vane to feed all the holes, as shown in Fig. 1. This plenum is fed from only one side, i.e. at the vane hub section. Tests were performed at coolant to mainstream blowing ratio (BR) values of 2.0, 3.0 and 4.0. BR is defined as follows:

$$BR = \frac{\rho_c U_c}{\rho_\infty U_\infty} = \frac{m_c}{m_\infty} \cdot \frac{A_\infty}{A_c} \qquad (1)$$

where A_c and A_∞ are the coolant exit section area and the mainstream cascade inlet section area, respectively.

To investigate the influence of density ratio DR, PSP tests were run both injecting nitrogen and carbon dioxide as coolant flow. When injecting CO_2, tests were run twice: first matching the same BR, then matching the same momentum flux ratio I, the latter defined as following:

$$I = \frac{\rho_c U_c^2}{\rho_\infty U_\infty^2} \qquad (2)$$

In both cases the reference nitrogen case is that at BR = 3.0. The cascade was tested in a continuously operating, suction-type subsonic wind tunnel for nozzle vane cascade (Fig. 2). The wind tunnel side walls are made of Plexiglas for optical accessibility. Ambient air is driven into the test section through a convergent inlet duct. The test section is connected to the fan through a diffusion section. Adjustable tailboards allow a fine tuning of exit flow condition to match periodicity constraints in the cascade central passages. Testing conditions prescribe an inlet Mach number Ma_1 of 0.063 and an exit isentropic Mach number Ma_{2is} of about 0.2. This testing condition is lower than the design inlet Mach number for this vane which is set at 0.12. Nevertheless, it was chosen in order to provide an acceptable operating condition for PIV measurements. As the focus of this investigation was on the leading edge region, the Mach number reduction was considered acceptable.

Figure 3 shows the approaching boundary layer measured $1.6C_{ax}$ upstream of the leading edge by means of a flattened Pitot probe. The assessment of boundary layer thickness is relevant for the present investigation, where coolant to mainstream interaction is analysed not only in the mid span region but also along the vane span, extending the measurement region up to the vane to end wall junction, where the horseshoe vortex is going to develop. This could influence the jet to mainstream mixing process in that region. Integral parameters are also reported together with mid span inlet turbulence intensity level in the stream wise direction measured by a single wire hot wire probe. Differently from previous testing conditions, due to accessibility constrains, the turbulence generator was not installed in the wind tunnel inlet section, resulting in a low inlet turbulence intensity level of 1.6%. The resulting boundary layer extends over about 14% of vane span, showing a transitional behaviour as indicated by a shape factor H_{12} of 1.7. As well known, much higher turbulence levels characterize the flow entering the first nozzle guide vane. As shown in [9], a high free stream turbulence promotes the main flow penetration through the coolant jets towards the vane surface, also influencing the unsteady jet behaviour. Again, the low turbulence operating condition was imposed by the PIV setup, requiring an optical access to the flow field for the laser sheet, that would have been compromised by the installation of the turbulent generator at the wind tunnel inlet section.

Cascade operating conditions were controlled monitoring the cascade inlet total P_{t1} and static pressure P_1 (by means of a 3-hole probe located $1.6C_{ax}$ upstream of the leading edge) and the downstream static pressure P_2 (31 pressure taps distributed over two pitches $0.45C_{ax}$ downstream of the trailing edge). The cooling system was first calibrated in order to define a relationship between the coolant mass flow m_c (orifice device) and coolant to mainstream pressure ratio P_c/P_1, where P_c (but also T_c) was measured by a pressure tap connected to the plenum realized inside of the vane (see Fig. 1). All subsequent tests, aero and thermal, were run setting the total pressure ratio corresponding to the desired BR value.

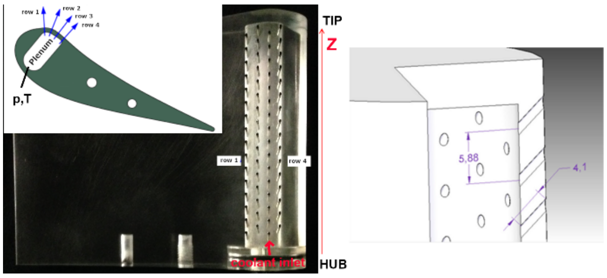

Fig 1. The showerhead cooling scheme (dimensions in mm).

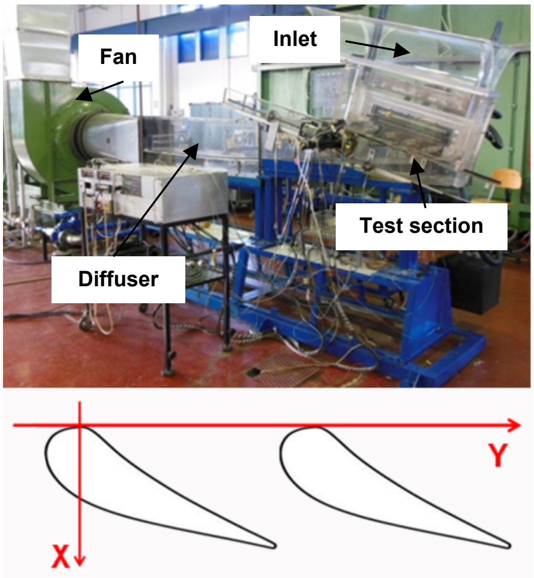

Fig 2. The wind tunnel and the cascade.

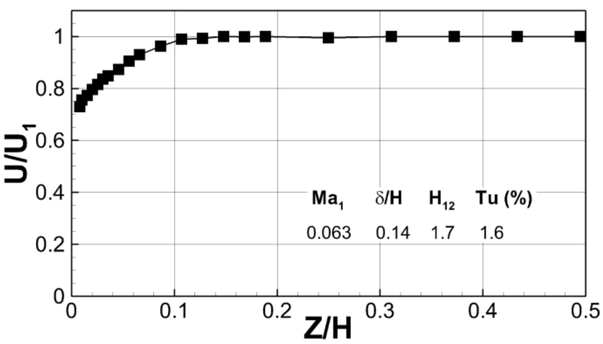

Fig 3. The approaching boundary layer ($X/C_{ax} = -1.6$).

2.2 Instrumentation

The wind tunnel and the cooled vanes were instrumented with pressure taps and thermocouples to control the operating conditions. Moreover, an instrumented vane was used to get the load distribution. Pressure taps and the 3-hole probe were connected either to Kulite XT series gauge pressure transducers or to a 48 channels rotary pressure scan (Scanivalve). Temperature signals were measured by T-type thermocouples. All signals were acquired using a HP 3852A D.A.C.U. unit (12bit resolution). All pressure transducers (FS of 0.34 bar) and T type thermocouples have been internally calibrated. Uncertainty on pressure measurement is about ± 10 Pa and that on temperature measurement is ± 0.1°C. During the calibration process of the cooling system, an orifice device was used to measure the injected mass flow m_c. This value was used, together with the main stream mass flow, to compute the blowing ratio BR, defined through eq. (1). The maximum uncertainty in the measured m_c value, calculated according to international standards for orifice devices (EN ISO 5167-2:2003(E)), was $\delta m_c = \pm 3.0\%$. The corresponding uncertainty in the BR value was ± 3.3% as a maximum.

A four beam, two color LDV system from DANTEC Dynamics was used to investigate the solid vane cascade in the mid span leading edge plane almost corresponding to plane 1-3c of Fig. 5. The probe was equipped with a 400-mm focal length front lens producing a measurement volume of 0.12 mm in diameter and of 2.5 mm in length. The probe was traversed both upstream and inside of the passage, with a grid spacing of 15 points per pitch in the tangential direction. At each location 10000 burst signals were acquired in coincidence mode, using sawdust smoke to seed the flow. The high number of acquired signals assured statistically accurate averages: based on a 95% confidence level, uncertainties of less than ±0.1% and ±1.4% for mean and rms values, respectively, have been obtained for a turbulence intensity level of 2%.

2.3 Pressure sensitive paints set-up

Film cooling effectiveness measurements in the leading edge region were performed using Binary Pressure Sensitive Paints by ISSI Inc. BinaryFIB paint is a dual-luminophor paint that contains two distinct luminescent dyes [25]. As well known, when the PSP paint is excited by a 400 nm light, two distinct signals are emitted: the first one at 560 nm is temperature dependent, while the second one, at 650 nm, is pressure and temperature dependent. As temperature influences the two signals similarly, their ratio results to be temperature independent. The sensitivity of BinaryFIB paint is about 0.6% per kPa and 0.03% per °C.

PSP thus measures the partial pressure of oxygen, as light emission from the luminescent dye is influenced by oxygen quenching: the higher the oxygen concentration (and its partial pressure), the lower the intensity of the emitted light. Following Stern-Volmer law, the following expression can be derived to quantify the relationship between light intensity and pressure [26]:

$$\frac{P}{P_{ref}} = a_0 + a_1 \cdot \frac{R_{ref}}{R} + a_2 \cdot \left(\frac{R_{ref}}{R}\right)^2 \quad (3)$$

where R_{ref} and R are the ratios of emission intensities from the two luminophors at reference pressure P_{ref} and pressure P respectively,

$$\frac{R_{ref}}{R} = \left(\frac{I_{ref}}{I}\right)_{650} \Big/ \left(\frac{I_{ref}}{I}\right)_{550} \tag{4}$$

while a_i are calibration coefficients. To be used for film cooling effectiveness measurement, the analogy between heat and mass transfer must be satisfied, allowing to compute η considering concentration instead of temperature to track the coolant at the wall [27]:

$$\eta = 1 - \frac{c_{O_{2,fg}}}{c_{O_{2,air}}} = 1 - \frac{1}{\left[1 + \left(\frac{P_{O_{2,air}}/P_{O_{2,ref}}}{P_{O_{2,fg}}/P_{O_{2,ref}}} - 1\right)\frac{MW_{fg}}{MW_{air}}\right]} \tag{5}$$

where $c_{O_{2,air}}$ and $c_{O_{2,fg}}$ are the O_2 concentration using air and a foreign gas not containing oxygen as coolant, respectively. MW_{fg} and MW_{air} are the molecular weight of foreign gas and air, respectively.

Heat/mass transfer analogy is surely true in case of fully turbulent flows, i.e. when the Lewis number is about one. This could not be always the case in the leading edge region. But the advantages of using a mass transfer technique instead of a heat transfer one in that region motivated the selection of PSP. In fact, PSP provides data unaffected by conduction and by curvature effects that instead strongly limit for example the accuracy of thermochromic liquid crystals (TLC) results.

Binary PSP were in-house calibrated using a sealed chamber where pressure can be varied between 1kPa and the ambient pressure under controlled temperature condition. The target surface sprayed with PSP is illuminated by a LED UV lamp operating in flash mode to minimize the aging effect of the PSP coating. A FlowSense EO 4M CCD camera with a 2048 x 2048 resolution and a 12bit sensitivity equipped with a multiple filter holder was used to get 50 frames for each pressure value. UV lamp and CCD camera were synchronized through the Timer Box of Dantec PIV system. The camera exposure time was set to maximize the signal to noise ratio of the PSP emitted light. The 50 images were then averaged to reduce the influence of noise. A further image, called Dark image, was acquired in atmospheric condition with the light switched off to be subtracted to any other acquired image. This is done in order to correct any CCD camera sensor defect. Figure 4 shows the calibration curve obtained in this study compared with the one proposed by the manufacturer. A good agreement between the two curves can be observed but for the low pressure region, probably due to different CCD camera characteristics.

The same illumination and image acquisition system was also used for cascade testing. Both the UV lamp and the CCD camera were located on one side of the wind tunnel, allowing to inspect about 70% of the vane span. To obtain the adiabatic film cooling effectiveness distribution, for each injecting condition 4 sets of images for each luminophor (and thus filter) were collected: the first one with both the light and the wind tunnel switched off (Dark image), the second one with only the light switched on (Reference Wind off Image), the third one injecting air as coolant and the last one injecting a foreign gas. In the present investigation nitrogen and CO_2 were used as foreign gas, resulting in a coolant to main stream density ratio DR of 1.0 and 1.5, respectively.

A perturbation analysis [28] was performed in order to compute the uncertainty in film cooling effectiveness values measured with PSP. CCD camera sensitivity and the accuracy of pressure transducer used for calibration (± 189.6 Pa) were considered. An uncertainty of $\delta\eta = \pm 0.5\%$ with $\eta = 0.7$ and of $\delta\eta = \pm 15.6$ % when $\eta = 0.1$ was computed. PSP results were also compared against TLC data from the same geometry and testing condition [29], showing a consistent behavior of the computed effectiveness in the investigated domain for variable BR. Nevertheless, TLC always overestimated the film cooling effectiveness levels in the near hole region, due to conduction and curvature effects.

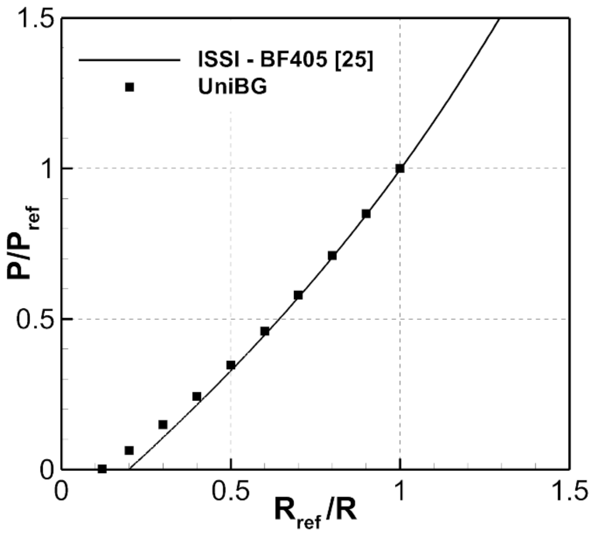

Fig 4. Binary PSP calibration curve.

2.4 Particle Image Velocimetry set-up

Two-dimensional Particle Image Velocimetry (PIV) technique was used to perform flow field measurements and flow visualizations on four planes located:

- in a chord wise direction, perpendicular to the vane surface and in correspondence of the 7th holes of rows #1 and #3 and the 7th holes of rows #2 and #4 (1-3c and 2-4c in Fig. 5);
- along the vane height, perpendicular to the vane surface and in correspondence of rows #1 and #4 (1s and 4s in Fig. 5).

The PIV setup included a 200 mJ double cavity Nd:Yag laser operating at a wavelength of 532 nm that generates the laser sheet necessary to illuminate the tracers particles seeded in the coolant flow by means of a Laskin nozzle seeding generator, a 12-bit CCD cooled camera with a resolution of 1024x1280 pixels, equipped with Nikkor lenses of 105mm focal length, and the related synchronization and acquisition system.

In order to be able to perform the image space positioning, image dewarping and perspective correction, a calibration target made of an orthogonal grid of black dots with a spacing of 1x1 mm was used. After data acquisition, the PIV images were processed using the commercial software PIVview from PIVTEC GmbH. A multi-size window refinement method was adopted in order to perform a cross-correlation between the two frames of each acquired image couple; Gaussian peak-fitting was adopted to perform the sub-pixel interpolation. Finally, the maximum displacement difference, primary to secondary correlation peak and minimum signal-to-noise ratio were adopted as vector validation criteria (refer to [30] for more details about the processing procedure).

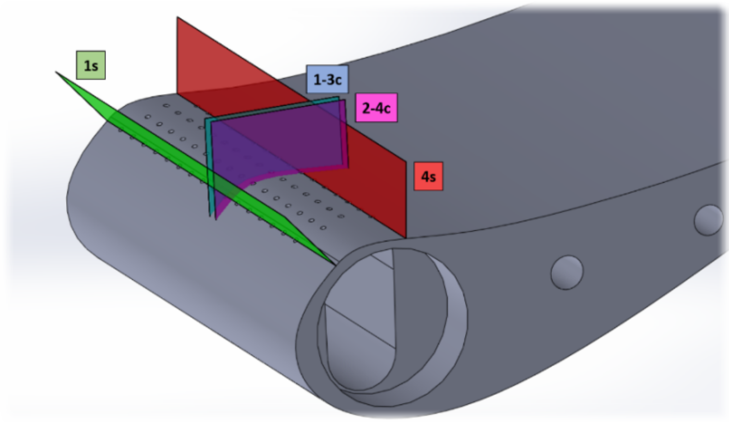

Fig 5. Position and nomenclature of PIV measurement planes.

In the following, only time averaged flow fields or higher order statistics will be presented. They are the results of the ensemble averaging of 1000 uncorrelated instantaneous samples. Their normalized errors (sampling error) can be computed from the theory of signal analysis [32] as follows:

$$\varepsilon_U = \pm \frac{Z_c}{\sqrt{N}} \frac{U_{rms}}{U} \qquad (6)$$

$$\varepsilon_{U_{rms}} = \pm \frac{Z_c}{\sqrt{2N}} \qquad (7)$$

where N is the number of samples, Z_c is the confidence coefficient, U is the mean velocity and Urms its rms velocity fluctuations. Due to the limited number of samples used to compute the flow statistics, the sampling error is larger than other error sources related to PIV [31] and therefore it can be considered as an upper bound estimate of the measurement uncertainty. Provided the value of Z_c=1.96 (for a confidence interval of 95%), eqns. (6) and (7) allow to estimate the measurement uncertainty all over the investigated areas. In particular, the uncertainty in the mean velocity turns out to be less than ±3% in most part of the flow fields, except for limited regions of very low velocity/high fluctuations at the boundaries of coolant jets. The normalized error in the rms velocity components from eq. 7 is limited to ±5% and this value applies over the whole measurement domain.

An additional comment is worth to be made about the data acquired in plane 4s, i.e. about row#4. At this vane location, the main stream is fully crosswise with respect to the measurement plane (this does not apply to plane 1s since its location is close to stagnation, as it will be possible to observe in Fig. 7); this can induce a parallax error in PIV data. However, parallax effect was minimized by the adoption of long focal length optics on the PIV camera and was also checked by a cross comparison of the data acquired in planes 4s, 1-3c, and 2-4c. Indeed, those planes share the same vertical (i.e normal to the vane surface) velocity component along their intersection line. The comparison of these velocity profiles (not shown for reason of brevity) turned out to be satisfactory with difference limited within the measurement uncertainty, so confirming negligible parallax errors in the 4s plane data.

3. RESULTS AND DISCUSSION

In the following, the leading edge flow structure without coolant injection is first described in order to provide a reference for the following discussion on the interaction between coolant and mainstream. Film cooling effectiveness maps measured with PSP technique at variable BR for the N_2 case and at matching BR and momentum flux ratio I for the CO_2 case are then presented and discussed, allowing to trace the coolant on the vane surface and to define the scaling parameter for engine condition. Off wall PIV results in the blade to blade planes and along the span are finally shown for the selected case of BR = 3.0. The whole data will support the understanding of the complex mixing process in the stagnation region. Finally, a selection of high speed flow visualizations will be presented, with the aim of gaining information on the unsteady jet behavior.

3.1 Uncooled vane results

Figure 6 shows the vane load distribution in the leading edge region, while Fig. 7 reports the contour plot of normalized main flow velocity (Vel_{xy}) in the stagnation region of mid span blade to blade plane with streamline traces. These last data were derived from LDV measurements. Normalization is made using the undisturbed approaching mainstream velocity U_1. The lack of data close to the vane surface is due to the need of preserving the Laser beams from intersecting the vane. In Fig. 6, s is the curvilinear coordinate tangent to the vane surface, positive along the pressure side and negative along the suction side; here it is normalized with the vane true chord C. Axial X and tangential Y coordinates in Fig. 7 are defined according with Fig. 2; they are normalized using the axial chord C_{ax} and the vane pitch S respectively. Figure 6 and 7 show that stagnation line is located very close to row#2. In particular, from the load distribution reported in Fig. 6 it seems that stagnation coincides with row#2. It has to be pointed out that, the total pressure used to compute the reported Ma_{is} value coincides with the highest pressure value measured with the instrumented vane. An uncertainty in the stagnation point position thus arises, as large as ±0.029 s/C, i.e. half the spacing between pressure taps. Considering this uncertainty, the slope of pressure distribution around the stagnation region and streamlines derived from LDV measurements (Fig. 7), it can be concluded that in the uncooled vane stagnation point is likely to occur somewhere in between row#2 and row#3, as shown by the dotted line extrapolated to the wall reported in Fig. 7. Moreover, it clearly appears that row#1 is located in a region of strong acceleration, whilst row#3 and row#4 position is on a slightly accelerating zone.

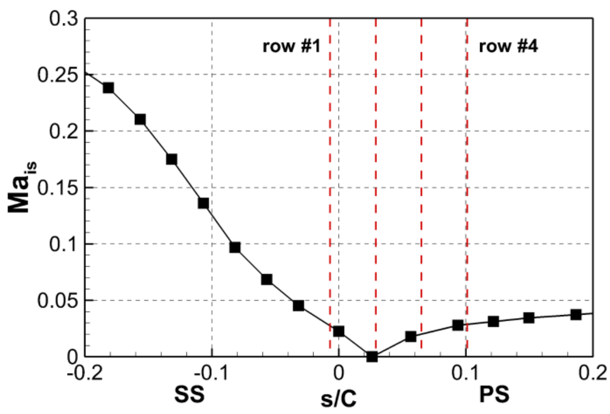

Fig 6. Vane load in the leading edge region.

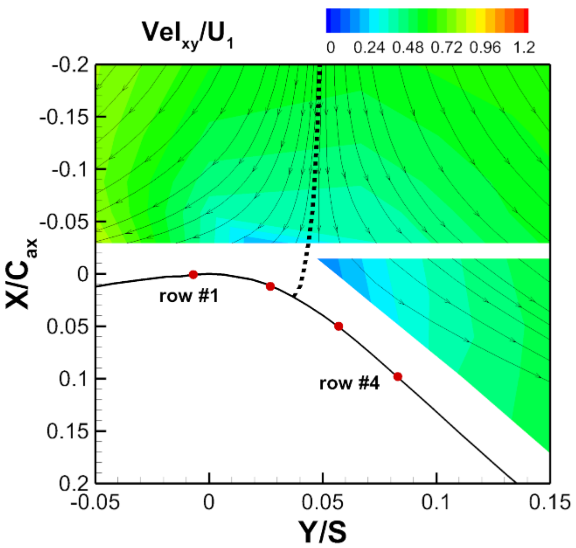

Fig 7. Mean velocity distribution in the stagnation region (*Z/H* = 0.5).

3.2 Film cooling effectiveness

Figure 8 reports adiabatic film cooling effectiveness contours obtained from PSP tests run with N_2 at varying BR from 2.0 up to 4.0. In all figures, coolant enters the vane at the hub (Z/H = 0) and holes are injecting coolant towards the tip

(*Z/H* = 1.0). In general, the vane thermal protection is highly non uniform along the span, especially along the pressure side and at high injection rates. Indeed, the hub section of the vane is poorly cooled, especially on the suction side. It progressively increases along the vane span thanks to the cumulative effect due to the hole injection angle toward the tip. Contrary to the uncooled vane load distribution, it seems that only row#1 contributes to the suction side cooling, with row#2 to #4 injecting coolant towards the pressure side.

At a low injection rate of BR = 2.0 (Fig. 8a), traces of coolant injected along the pressure side are evident even at low elevation in the spanwise direction, with a quite uniform thermal protection along the pressure side starting from Z/H = 0.1. Worth to mention are the jet traces emerging from row#2, confirming that this row is injecting towards the pressure side. As a consequence, the leading edge suction side results to be cooled just by row#1. Coolant ejected through row#1 and row#2 is already detached from the wall: it is then diverted towards the vane surface by the approaching main flow. Jets traces emerging from both row#3 and row#4 can be easily detected especially at high elevation, where jet to jet interaction along the span and row to row interaction along the stream wise direction both contribute in keeping the coolant attached to the wall.

Increasing BR up to 3.0 (Fig. 8b) results in an increase of effectiveness in the near hole exit region and in a cooled triangular region along the span, consistent with a significant influence of coolant momentum in the spanwise direction. Coolant in fact can travel further along the span, before turning in the stream wise direction under the influence of the main flow. This results in a loss of protection at small radii and in an increase in the thermal coverage at larger elevation. Increasing injection up to BR = 4.0 (Fig. 8c), results in a reduction of coolant persistency along the pressure side, due to the higher accumulation towards the tip induced by the coolant high span wise momentum. A beneficial effect is instead observed on the front suction side, where jet reattachment is evident closer to the hub, up to Z/H = 0.1, probably due to an increased hole to hole interaction along the span.

Figure 9 shows the adiabatic film cooling effectiveness contours obtained from PSP test run with CO_2 as foreign gas at the matching blowing ratio (BR = 3.0) and the matching momentum flux ratio (I = 9.0) of N_2 case reported in Fig. 8b (BR = 3.0). Film cooling effectiveness traces become wider and longer for cases with CO_2 as coolant. These findings are in good agreement with the literature [32] and with data measured with TLC technique on the same geometry [29]. First focusing on the suction side, the thermal footprint on the vane clearly shows a jet separation downstream row#1 followed by reattachment that happens closer to the holes in case of using coolant with a higher density. At *BR* = 3.0 with N_2 and CO_2, a certain periodicity in the coolant footprint along the span can be observed starting from the 4th hole from the hub (corresponding to *Z/H* = 0.24). Considering the same momentum flux ratio, the appearance of this periodic behavior is anticipated down to *Z/H* = 0.1, i.e. right after the second hole.

Moving to the pressure side, a quite good thermal protection is obtained with jet traces that can be identified downstream of row#2 over most of the span, especially when matching the momentum flux ratio which provides a higher amount of coolant into the mainstream. It should be mentioned that a periodic condition along the span is never reached on the pressure side.

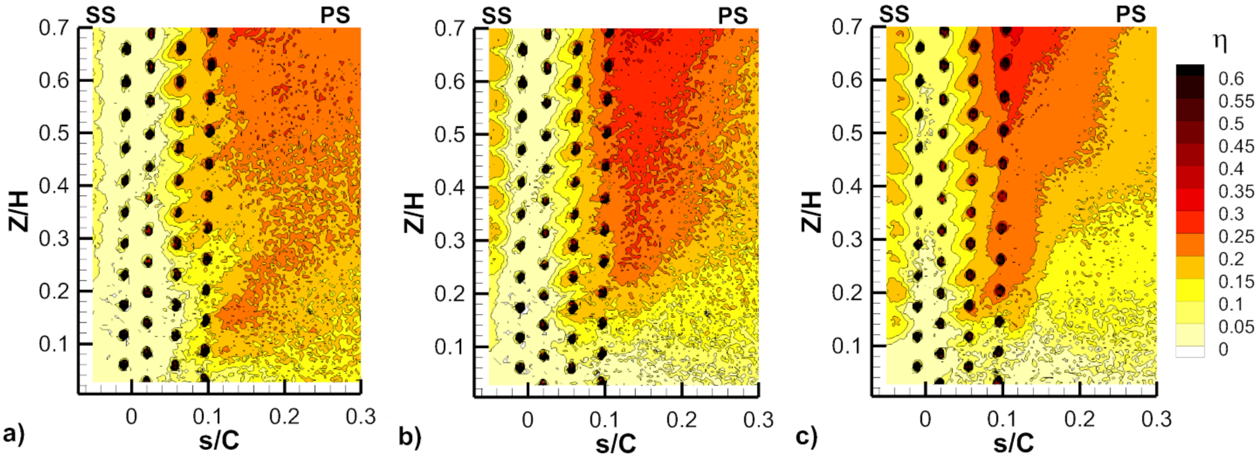

Fig 8. Film cooling effectiveness η distributions (DR=1.0) for: a) BR=2.0, b) BR=3.0 and c) BR=4.0.

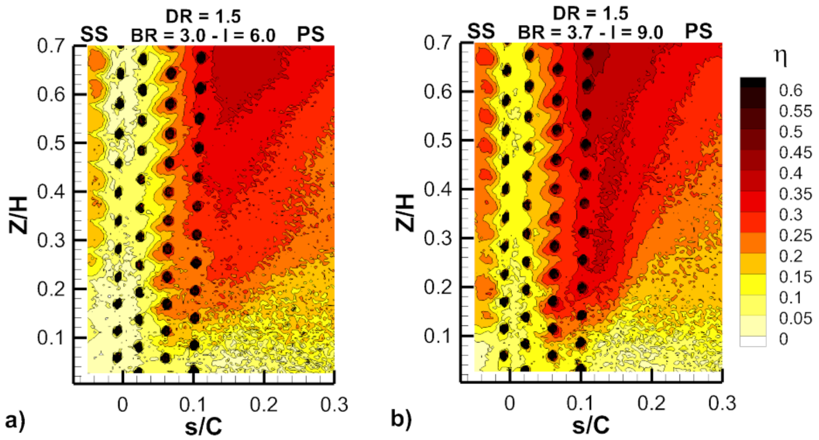

Fig 9. Film cooling effectiveness η distributions for: a) DR=1.5, BR=3.0, I=6.0 and b) DR=1.5, BR=3.7, I=9.0.

Furthermore, Fig. 10 gives the laterally-averaged film cooling effectiveness distributions along the vane span portion shown in Fig. 8 and 9 for all the cases. First considering the impact of BR on the laterally averaged film cooling effectiveness distributions measured at DR = 1.0 (Fig. 10a), an increase of BR from 2.0 to 4.0 is beneficial for the front suction side and in between the holes. A quite different behavior characterizes the pressure side where two distinct regions can be identified: a first zone extending from row#4 down to s/C = 0.1, where an optimal injection condition at BR = 3.0 can be identified, and the downstream region, where the thermal protection decreases with rising BR. These behaviors result from the complex interaction between coolant jets with progressively increasing momentum along the span and the mainstream. In fact, in the near hole exit region, a high span wise coolant momentum is expected to promote the interaction between holes belonging to the same row. A reduced span wise momentum is instead expected to promote the interaction between jets coming from different rows, hence coolant persistency in the stream wise direction.

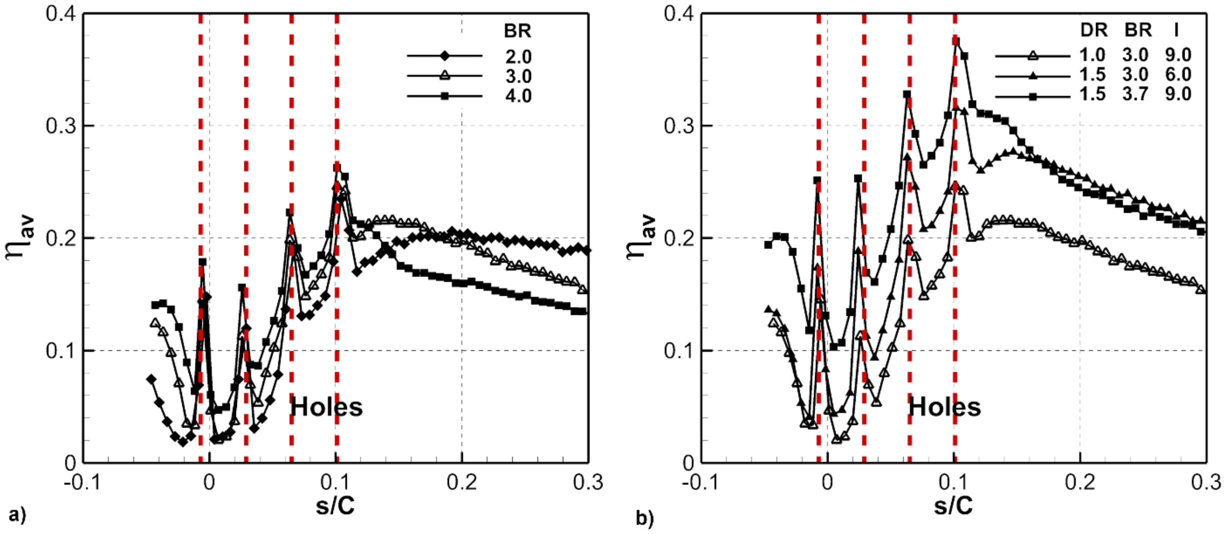

Fig 10. Laterally-averaged film cooling effectiveness profiles: a) for variable BR at DR = 1.0 and b) for variable DR.

Shifting attention to the impact of DR (Fig. 10b), laterally-averaged film cooling effectiveness is higher along the pressure side for either cases with heavier density coolant, due to the lower coolant momentum which leads to coolant higher tendency to adhere to the leading edge. More specifically, downstream of the holes (s/C >0.1), coolant with higher density ratio shows the highest effectiveness since jets velocity is reduced as well as coolant penetration into the mainstream which is notable from Fig. 9a. Furthermore, the maximum effectiveness occurs in the third case (DR=1.5, BR=3.7, I=9) just downstream injection because of higher BR. In this case in fact, due to the higher coolant density and also the cumulative effect, jets are still attached to the surface which results in a higher effectiveness. This is consistent with results presented in fig. 9b. Shifting attention to the hole's region and along the front suction side, a quite good matching between low and high DR cases is observed when considering the same BR. Matching the momentum flux ratio instead gives larger laterally averaged effectiveness all over this region. These findings are consistent with Cutbirth and Bogard [33] results, showing a better superposition of results at different DR when matching BR rather than I. This was true at low BR. Increasing BR, the difference between low and high density ratio cases also increased, with a systematic under-prediction of η_{av} when injecting at DR = 1.

3.3 Flow field characterization at constant Ma_1 = 0.063 and BR=3

3.3.1 Mean flow field in the blade-to-blade planes.

The BR = 3.0 injection case was considered worth to further investigation from the aerodynamic point of view. In fact, it gives the best thermal performance for this cooling scheme, i.e. a good compromise between coolant consumption and surface thermal protection, especially in the near hole exit region. Moreover, as significant jet liftoff phenomena were evidenced by PSP measurements, as well as non-negligible jet to jet interactions, this injection case was considered to be an interesting test case for CFD validation. Worth to mention is that the only data available in the literature [9] were obtained at BR = 2.0, where jet separation was less relevant.

Figure 11 reports the contour plots of the time averaged in plane normalized velocity (Vel_{xy}) and the corresponding stream tracers resulting from PIV measurements in planes 1-3c and 2-4c (Fig. 5). The time averaged interaction between the coolant flow and the main stream is well highlighted by the path of the stream tracers which, close to the vane surface, show a wavy pattern with impingement and separation from the surface, in particular on the vane PS. Similarly, the velocity distribution of the flow field around the leading edge is characterized by the existence of local spots of higher or lower velocity (with respect to the main stream). In the majority of cases these spots do not emerge from the holes but are detected few millimeters away from the vane surface. A clear example of this are the two low velocity regions that are found on the two sides of the approaching stagnation stream trace (dotted line in Fig 11) in both the investigated positions and the two high velocity regions that are similarly found below these regions, especially in plane 2-4c, but still off the wall. Most likely, these are the footprints of the coolant jet arising from the holes pertaining to row #1 and row #2 and ejected at a lower Z/H position with respect to the measurement planes, consistently with the injection direction towards the vane tip. It is therefore clear that jets from the first two rows tend to penetrate the main stream so failing to provide an effective thermal protection immediately downstream the injection point, as seen from the PSP results previously commented. Similar high velocity spots can be identified also close to row#3 and #4 along the front pressure side, indicating the presence of coolant jets emanating from holes located at lower span wise elevation. A lower interaction with the mainstream takes place here: no low velocity regions are observed above the jet traces, indicating that the mainstream just flows over the coolant, far from the vane surface, in agreement with the good thermal protection observed in this region.

The interaction of the coolant jets with the mainstream has also the effect of modifying the stagnation line position. In the uncooled vane the stagnation point was found downstream of row #2 (see Figs. 6 and 7), while for the cooled vane case the stream traces path clearly show that stagnation moves towards the suction side: it can be localized in between row #1 and row #2, as also confirmed by the very low velocity values measured in that region. This is consistent with

Bohn et al [14] results, showing a change in the stagnation position at high blowing ratios, and with Polanka et al. [9] findings, reporting as well a slight shift in the stagnation line as a result of jet to mainstream interaction.

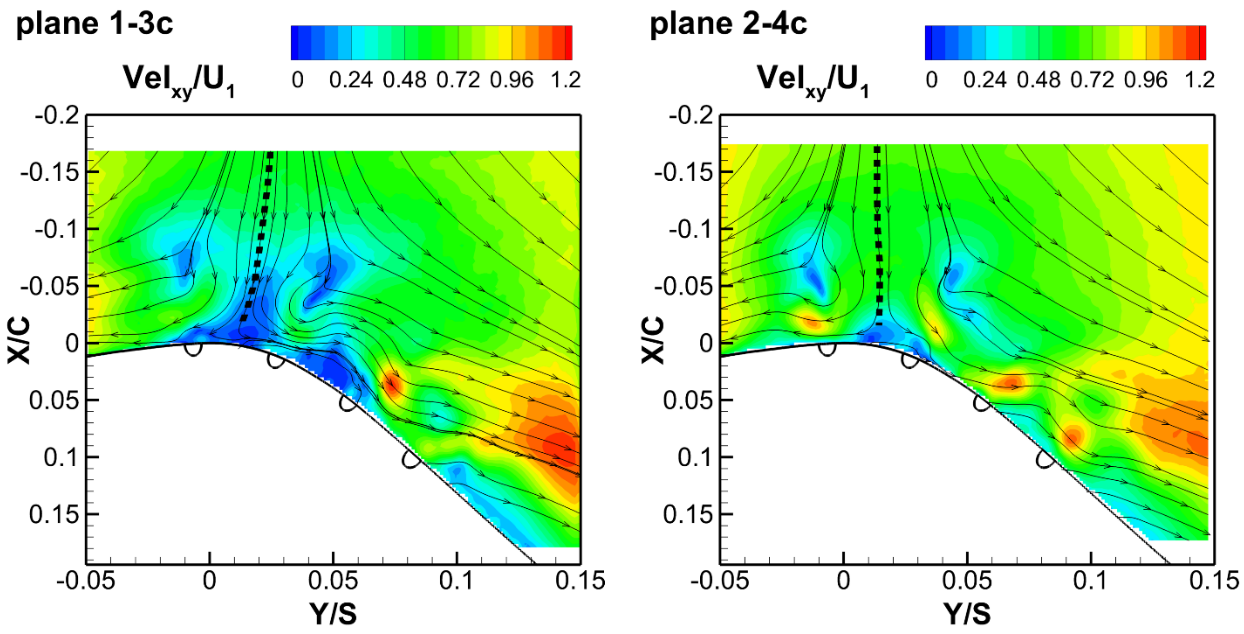

Fig 11. Mean normalized in plane velocity contour and stream tracers in planes 1-3c and 2-4c.

The complex interaction between the coolant and the main flow is also documented by the plots of mean flow vorticity and rms velocity components. Figure 12 reports the in plane component of the vorticity vector ($vort_{xy}$) computed by the time averaged axial (U_x) and tangential (U_y) velocities in both 1-3c and 2-4c planes. In both cases, regions with local positive or negative high vorticity values are found not only near the vane surface but also some millimeters off the wall and are associated to the curvature of the coolant jets by the main stream (and vice versa). For example, row#1 near flow field is dominated by the presence of two vortical structures: one rotating counterclockwise close to the hole exit and one rotating clockwise at higher elevation. The opposite takes place when looking at row#2. The intensity and position of these vortices changes when moving between plane 1-3c and plane 2-4c, according with a different distance from the hole exit. Something similar also takes place along the pressure side, even if further vortical structures of reduced intensity can be identified off the wall. These vortices are traces of the interaction with jets injected at a lower elevation. These flow modifications are strictly related to the jet trajectories that are in turn affected by the distance between the measuring plane and the hole and the jet to mainstream momentum ratio both in the stream wise and span wise directions. These data indicate a very complex 3D coolant to mainstream as well as jet to jet interaction with vortical structures that significantly change also depending on the spanwise position.

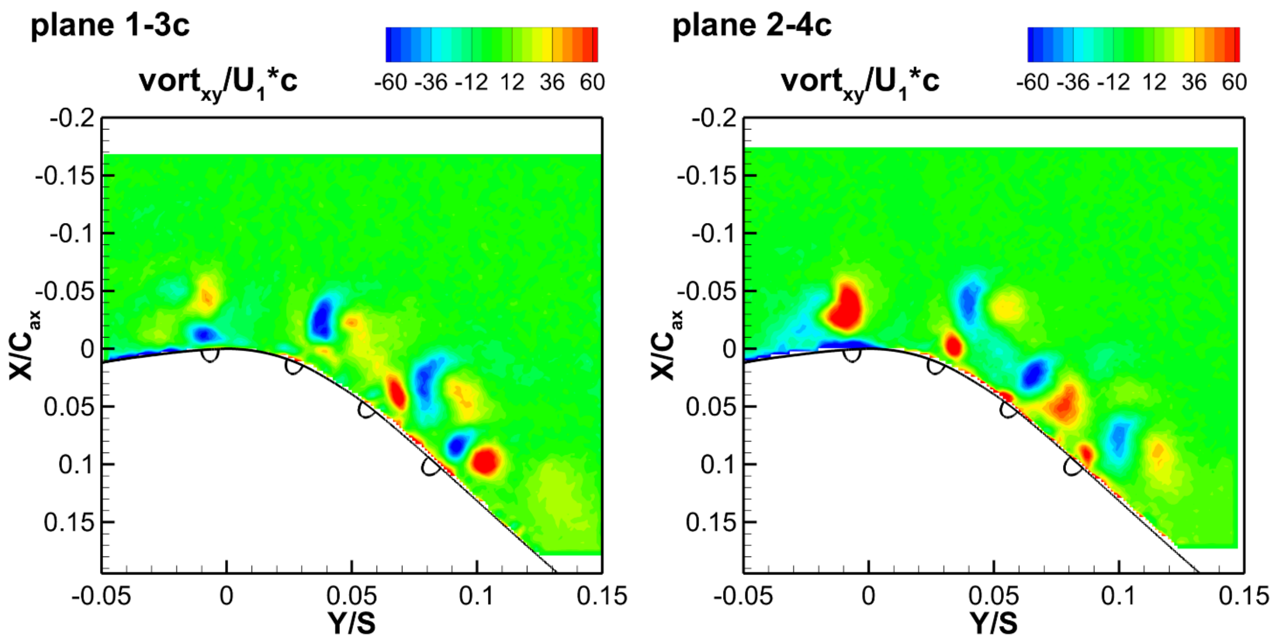

Fig 12. In plane component of the normalized mean vorticity in planes 1-3c and 2-4c.

The intensity of the diffusion and mixing process of the coolant inside and with the main stream can be appreciated by looking at the rms velocity components in Fig. 13. These data are reported for the 2-4c plane only since a similar behavior can be found also in plane 1-3c. Velocity fluctuations above 30% of the upstream velocity U_1 can be found all inside a region about $0.1X/C_{ax}$ wide and that surrounds the whole investigated leading edge region. Inside this flow region, local spots of even higher fluctuations (in both directions) can be found, unevenly distributed just on top or downstream the injection points, so giving a first indication of the strong anisotropic character of the turbulent process that takes place. The extension of this high turbulence region also gives an idea of how far coolant jets penetrate into the mainstream. The presence of huge velocity fluctuations supports the existence of a highly unsteady mixing process between coolant and mainstream. Worth to mention are the high rms values measured for row#1 and #2, the ones mostly affected by jet liftoff phenomena. A smoother mixing process instead characterizes both row#3 and #4, where coolant injection takes advantage of the cumulative effect with jets more attached to the wall. Again, some turbulence spots can be still identified at higher distance from the vane surface, tracing the mixing of jets injected at lower spanwise positions.

Similar turbulence levels were also reported by Polanka et al. [9] even at a lower injection condition of BR = 2.0. The local low values of rms_{Uy} measured in between row #1 and row #2 is another confirmation about the modified location of the stagnation point with respect to the uncooled vane case.

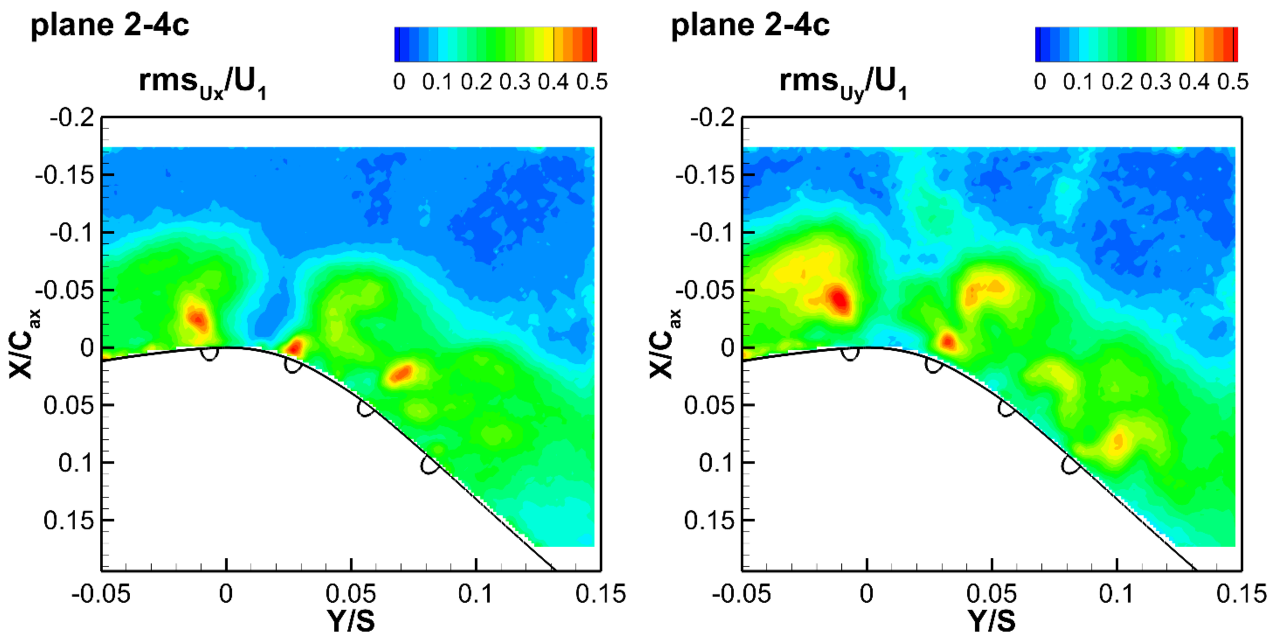

Fig 13. Normalized fluctuating velocity components in plane 2-4c: tangential (left) and axial (right) components.

3.3.2 Mean flow field in the spanwise planes

The blade to blade investigation has shown that coolant to mainstream interaction in such a showerhead cooling system is highly 3D. Hence a better and more complete description of this complex flow behavior can be gained by looking at the results obtained on the measurement planes aligned with the vane span and normal to the vane surface, located in correspondence of row #1 and row #4 (see Fig. 5).

Figures 14, 15, and 16 report the contour maps in planes 1s and 4s of the time averaged in plane velocity (Vel_{nz}), time averaged in plane vorticity component ($vort_{NZ}$) and rms velocity components, respectively. To have a closer look at coolant to mainstream interaction, two regions have been extracted and reported in Fig. 17: the region extending from Z/H = 0.4 to 0.52 for plane 1s and those from Z/H = 0.46 to 0.58 for plane 4s. These two regions were selected in the near mid span zone looking for a periodic flow condition along the span, possibly unaffected by light reflection related problems.

Figure 14a reports the time averaged in plane velocity (Vel_{nz}) and the corresponding stream traces measured in plane 1s. Coolant flow displacement towards the vane tip consequent to the selected 45° injection angle is well highlighted by the stream traces path. The velocity distribution shows a wide region of velocity deficit near the hub, while moving towards the tip footprints of coolant jets are well captured. Data in Fig. 17a show how high speed regions corresponding to the coolant jets are located above the wall low velocity region, indicating that jets liftoff the wall and then bend towards the vane tip. Actually, jet penetration into the mainstream is quite relevant, with its influence extending up to about 6D off the wall. This is not the case for plane 4s (Figs. 14b and 17b) where jets appear less intense and more diffused. The reason of this is twofold:

- at location of plane 4s the main flow velocity is aligned cross wise with respect to the measurement plane (see the stream tracers path in Fig. 11); the jets cores will therefore cross the measurement plane, i.e. their principal velocity cannot be measured in this plane;
- the accumulation of coolant from the upstream points of injection (row #2 and row #3) that contributes to the establishment of the coolant layer highlighted by the region of higher velocity that extends up to about N/D=8 from the vane pressure side.

The location of plane 4s, more downstream of stagnation with respect to plane 1s, allows the identification of the pressure side horseshoe vortex branch near the hub end wall junction (Fig. 14b). However, its presence does not prevent the first holes to discharge the coolant, as seen by the velocity plume in the contour map.

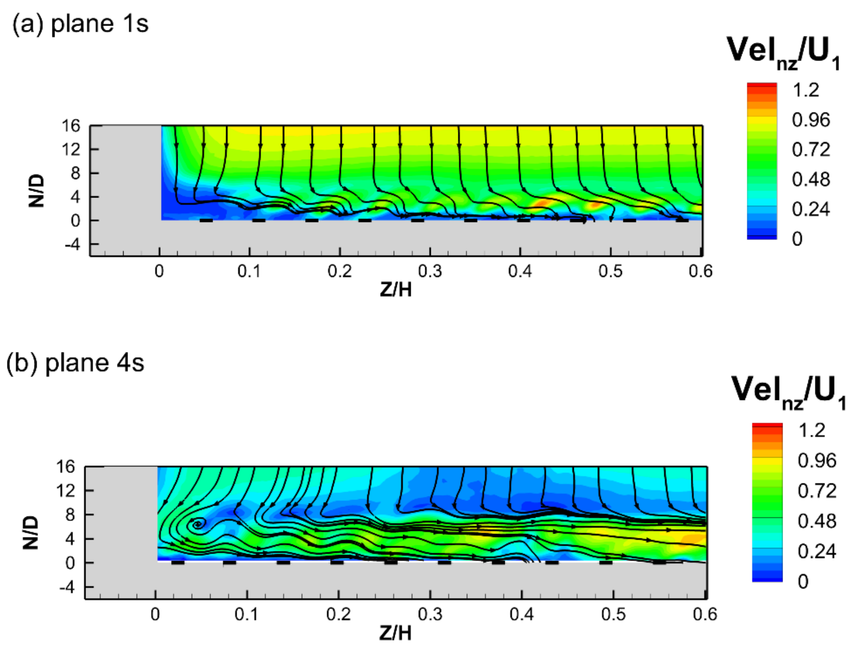

Fig 14. Mean normalized in plane velocity contour and stream tracers in planes 1s (a) and 4s (b).

The commented mean flow behavior for both row #1 and row #4 is consistent with the PSP results, where: higher η is observed moving towards the tip and far downstream row #3 and row #4; poor effectiveness values are measured close to the end wall and in particular for row #1.

In plane 1s the jet interaction with the main flow is well captured by the vorticity values reported in Figs 15a and 17c: an alternation of highly positive and negative vorticity peaks confirms the strong penetration of the coolant in the main flow, i.e. the liftoff of the jets from row#1. In addition, and consistently with the effectiveness distribution of above, the first hole close to the end wall does not supply appreciable coolant flow and the second one much less than the successive holes (see Fig. 15a). In plane 4s jets appear weaker in terms of vorticity than in the other plane (Figs. 15b and 17d), but this is again to be ascribed to the orientation of the main flow, as commented above about the results in Fig. 14. Nevertheless, it is possible to observe the regular pattern of the jets near the vane surface, while the negative vorticity spots located at N/D about 8 are due to the interaction of the main flow with the coolant ejected from the upstream rows. In fact, according with PSP results and with PIV data measured on the blade to blade plane, rows from #2 to #4 are injecting towards the pressure side, with only row #1 contributing to the cooling of the suction side. The vorticity distributions in plane 4s reflects this behavior, showing weak traces of the preceding rows.

Contour plots of rms velocity components are provided in Fig. 16 and 17e-h. As for the data in the blade-to-blade planes (Fig. 13), a remarkable anisotropy is found by comparing the two components, with the highest rms levels found in the spanwise component in plane 1s, in agreement with [9]. Fluctuations enhancement is generally observed in both measurement planes while moving towards the tip, the lowest flow agitation being detected close to the end wall, in particular for the first row (plane 1s, Figs. 16a, 16c), once again confirming the thermal behavior.

The detailed views of Fig.17 allow to get some other important confirmations. In plane 4s (Figs. 17f and 17h), both rms components distributions show local maxima close to the vane surface ($N/D<3$) and at higher elevation ($5<N/D<8$) confirming that: jets from row#4 tends to remain attached to the surface; at the location of this measurement plane jets from previous rows contribute to the formation of a coolant layer that extends up to about N/D=8. These two features contribute to a satisfactory thermal protection immediately downstream of row#4 (see data at BR=3 in Fig. 10a). This is not the case for plane 1s (Fig. 17e and 17g) where very low velocity fluctuations are detected close to the wall and in between the jets, again consistently with a jet liftoff behavior. Finally, both investigated planes show a strong jet to jet interaction along the span. On the pressure side, this is coupled with a strong jet to jet interaction even in the streamwise direction, resulting in a very complex flow emerging from the front pressure side. The subsequent strong acceleration will contribute in keeping this flow confined to the wall, in the meanwhile speeding up the aerodynamic mixing process.

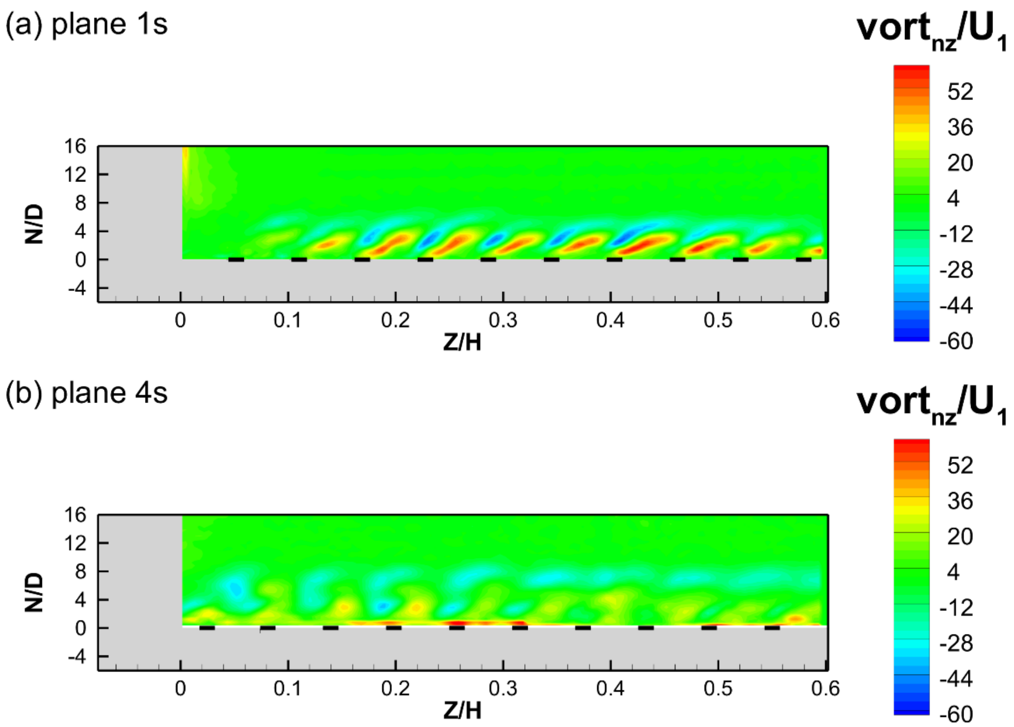

Fig 15. In plane component of the normalized mean vorticity in planes 1s (a) and 4s (b).

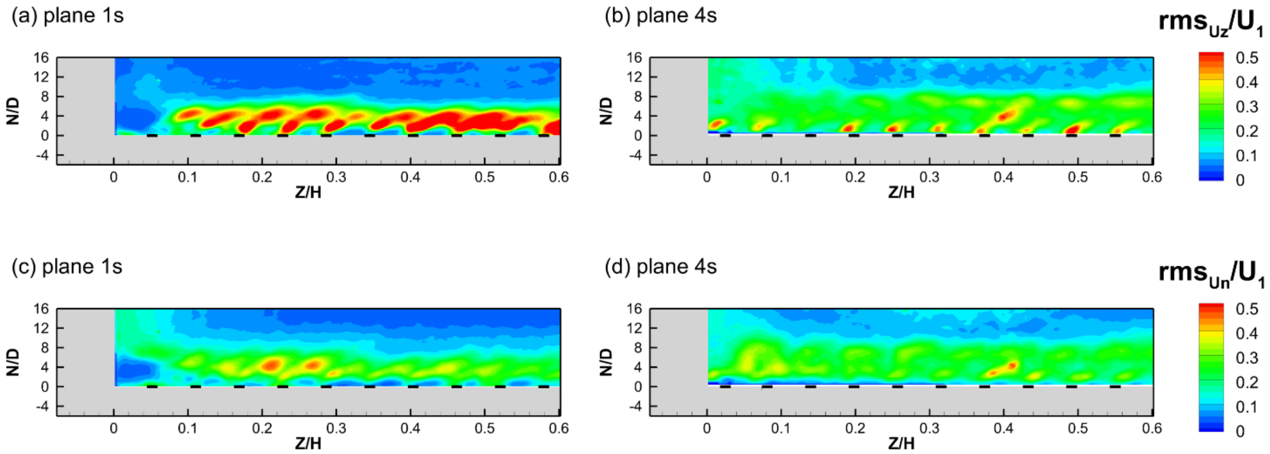

Fig 16. Normalized fluctuating velocity components in planes 1s and 4s: spanwise (a-b) and normal to the wall (c-d) components.

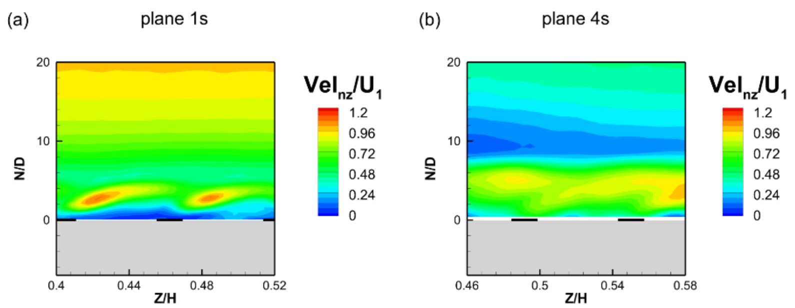

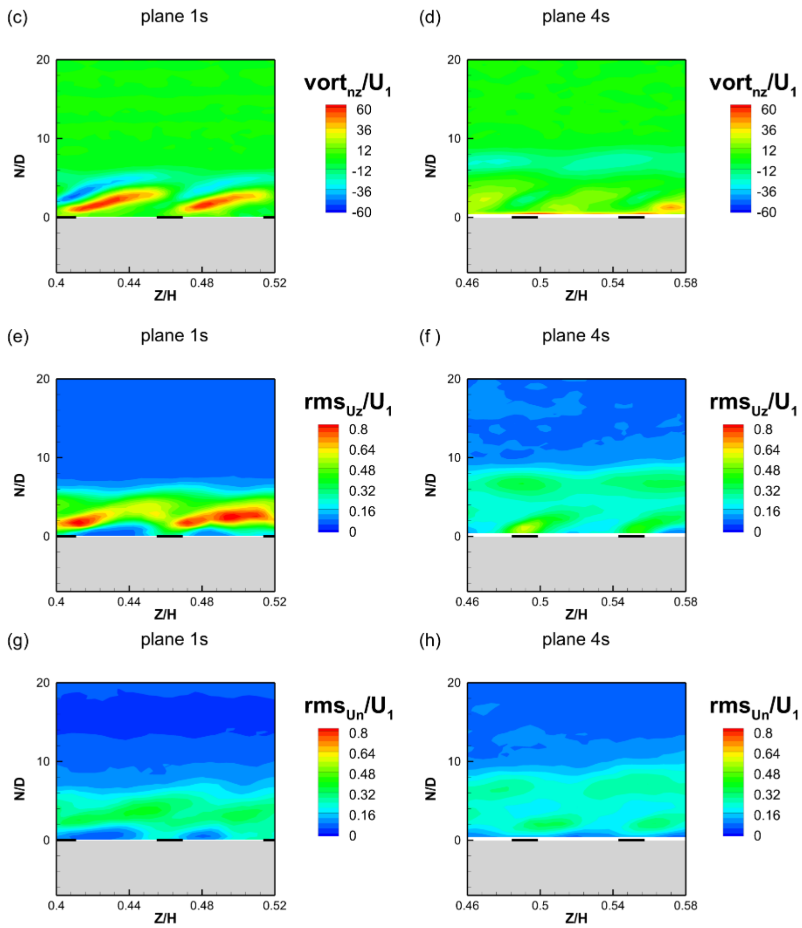

Fig 17. Normalized mean and RMS velocity and vorticity contours in planes 1s and 4s about the mid span region.

3.5 Cooling jet unsteady behavior

In order to understand more about the upstream movement of the stagnation point previously commented and the huge levels of fluctuating velocity components, a closer look to the instantaneous flow fields acquired in plane 1-3c and 2-4c for the BR value of 3.0 was carried out. This allowed to put in evidence the existence of a very complex flow behavior, intrinsically unsteady. Figure 18 reports successive instantaneous flow fields acquired in plane 2-4c at the sample frequency of 4Hz. Velocity vectors are superimposed to the vorticity map (in plane component), and for each flow map, the first frame of the corresponding PIV image pair is reported. The PIV images have been digitally manipulated in order to highlight the coolant flow (PIV seeding) and enable a better comprehension of the phenomena.

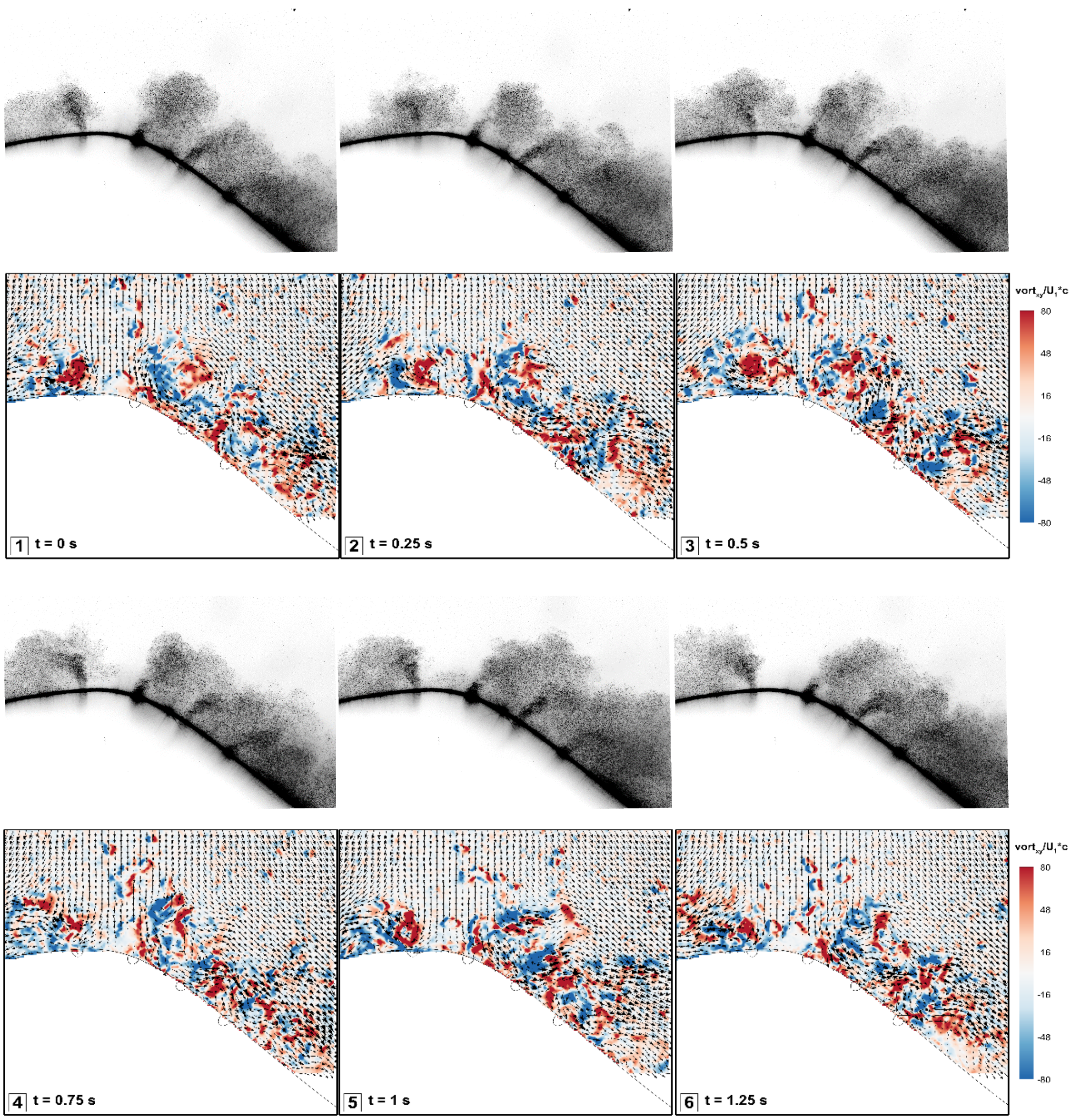

Fig 18: Instantaneous PIV frames and vorticity fields in plane 2-3c.

The first frame shows a situation in which a large stagnation region is located in between row #1 and row #2. In that region, flow velocity and therefore instantaneous vorticity is practically zero and the image shows no traces of coolant with jets 1 and 2 clearly moving towards the suction and pressure side, respectively. Moving to the next frame, 0.25s later in time, the stagnation region moves closer to the second row of holes and the main stream seems to reach the vane surface even downstream of this row. On top of the first hole a large and coherent vortical structure is captured. This latter brings coolant from the first jet towards the pressure side, as it is possible to observe from the PIV image. Moving further in time (frame 3 of Fig. 18), the vortical structure on top of the first row of holes becomes even larger, coolant is still present in between row #1 and row #2 and the stagnation point is found still closer to the second row. Frames 4 to 6 shows a situation that progressively tends to restore the initial one, with jets 1 and 2 that move towards suction and pressure sides and the stagnation point located in between.

The analysis of above is purely qualitative; unfortunately, due to the limitation in the repetition rate of the available PIV system, it was not possible to track in time the flow evolution. However, on the full population of instantaneous velocity fields, a proper orthogonal decomposition (POD) analysis was performed. This technique is used in fluid dynamics to extract dominant structures in the spatial domain and to investigate transient behavior. The POD results did not show any dominant mode in the flow, consistently with spectral analysis performed on LDV data where no dominant frequency content was observed, so confirming the random nature of the mixing phenomena between the coolant and the main flow.

4. CONCLUSIONS

The results of this combined aerodynamic and thermal investigation allowed to get a comprehensive view of the complex flow phenomena related to jet to mainstream mixing process in the showerhead leading edge region. Setup constraints imposed by PIV technique forced the selection of a cascade operating condition characterized by low inlet Mach number, low inlet turbulence intensity level and low coolant to mainstream density ratio of 1.0. To investigate the impact of BR and DR on showerhead cooling a sensitivity analysis on the adiabatic film cooling effectiveness distribution over the leading edge region was carried out by Binary PSP technique. This sensitivity analysis confirmed that matching BR is still the best choice at relatively high BR values, even with some limitations. A displacement of stagnation towards the suction side was observed at all injection conditions, with most of the rows of holes injecting along the pressure side and only one row contributing to the protection of the front suction side. Moreover, relevant liftoff phenomena were detected close to stagnation, with the thermal protection progressively increasing with BR in the near hole exit region and decreasing along the pressure side. The injection condition of BR = 3.0 was considered a tradeoff between thermal performance and coolant consumption. This condition was then considered worth of further investigation of the 3D unsteady nature of coolant to mainstream interaction. In this context, the PIV investigation performed on different planes gave an overview of the 3D flow field in the stagnation region as well as information on the turbulence characteristics and on the unsteady behavior of jet to mainstream mixing process. In particular, consistently with the literature, these data confirmed a displacement of the stagnation line towards the suction side induced by coolant injection. Three of the rows contribute to the coolant of the pressure side, while only one row injects coolant to the suction side, consistently with PSP data. Moreover, jets exiting the first row on the suction side are separated from the wall and then reattach at a certain distance along the suction side. This was coupled with huge values of all rms velocity components, especially in the span wise direction, with a high degree of anisotropy. Jet separation is still evident in the second row (the first one injecting along the pressure side), while the cumulative effect prevents the coolant ejected from the following rows to lift off the wall, resulting in a better thermal protection along the pressure side. High levels of turbulence have been detected even in that region, due to the strong jet to jet and jet to mainstream mixing process. Neither along the suction side, nor along the pressure side a true periodic flow condition is established in the radial direction, supporting the necessity of considering the full vane span, when performing CFD simulations. The inspection of sequences of PIV instantaneous frames also allowed to demonstrate the unsteady nature of showerhead coolant injection, even if no coherent structures could be identified, supporting the random nature of mixing process. Finally, the results presented in this paper will be useful for CFD validation.

References

[1] Wadia, A. R., and Nealy, D. A., 1985, Development of a Design Model for Airfoil Leading Edge Film Cooling," ASME Paper No. 85-GT-120.

[2] Reiss H., Bolcs A., 2000, Experimental study of showerhead cooling on a cylinder comparing several configurations using cylindrical and shaped holes, J. Turbomach., 122, pp. 161-169.

[3] Lu Y., Allison D., Ekkad S. V., Influence of Hole Angle and Shaping on Leading Edge Showerhead Film Cooling, ASME Paper GT2006-90370.

[4] Cruse, M. W., Yuki, U. M., and Bogard, D. G., 1997, Investigation of Various Parametric Influences on Leading Edge Film Cooling, ASME Paper No. 97-GT-296.

[5] Mehendale A. B., Han J. C., 1992, Influence of high mainstream turbulence on leading edge film cooling heat transfer, J. Turbomach., 114, pp. 707-715.

[6] Newman A., Xue S., Ng W., Moon H. K. and Zhang L., Performance of a Showerhead and Shaped Hole Film Cooled Vane at High Freestream Turbulence and Transonic Conditions, ASME Paper GT2011-45142.

[7] Polanka M. D., Witteveld V. C., Bogard D. G., 1999, Film cooling effectiveness in the showerhead region of a gas turbine vane Part I: Stagnation region and near-pressure side, ASME paper 99-GT-48.

[8] Witteveld V. C., Polanka M. D., Bogard D. G., 1999, Film cooling effectiveness in the showerhead region of a gas turbine vane Part II: Stagnation region and near-suction side, ASME paper 99-GT-49.

[9] Polanka M. D., Cutbirth J. M., Bogard D. G., 2002, Three component velocity field measurements in the stagnation region of a film cooled turbine vane, J. Turbomach., 124, pp. 445–452.

[10] Nathan, M. L., Dyson, T. E., Bogard, D. G., Bradshaw, S. D., 2013, Adiabatic and Overall Effectiveness for the Showerhead Film Cooling of a Turbine Vane, J. Turbomach., 136(3), p. 031005.

[11] Albert J. E., Bogard D. G., Cunha F., 2004, Adiabatic and overall effectiveness for a film cooled blade, ASME paper GT2004-53998.

[12] Cutbirth J. M., Bogard D. G., 2001, Thermal field and flow visualization within the stagnation region of a film cooled turbine vane, ASME paper 2001-GT-0401.

[13] Bogard D. G., Thole K. A., 2006, Gas Turbine Film Cooling, AIAA Journal of Propulsion and Power, 22(2), pp. 249-271.

[14] Bohn D. E., Becker V. J., Rungen A. U., 1997, Experimental and Numerical Conjugate Flow and Heat Guide Vane. ASME Paper No. 97-GT-15.

[15] York, W.D., Leylek, J.H., 2002. Leading-edge film-cooling physics: Part I – adiabatic effectiveness. In: Proceedings of ASME Turbo Expo, GT2002-30166. The Netherlands, Amsterdam.

[16] York, W.D., Leylek, J.H., 2002. Leading-edge film-cooling physics: Part II – Heat Transfer Coefficient. In: Proceedings of ASME Turbo Expo, GT2002-30167. The Netherlands, Amsterdam.

[17] Ledezma, G.A., Laskowski, G.M., Dees, J.E., Bogard, D.G., 2011. Overall and adiabatic effectiveness values on a scaled up simulated gas turbine vane: Part II – numerical simulations. In: Proceedings of ASME Turbo Expo, GT2011-46616, Vancouver, Canada.

[18] Heidmann, J. D., Rigby, D. L., and Ameri, A. A., 1999, A Three-Dimensional Coupled Internal/External Simulation of a Film-Cooled Turbine Vane, J. Turbomach., 122(2), pp. 348–359.

[19] Dyson, T. E., Bogard, D. G., and Bradshaw, S. D., 2012, Evaluation of CFD Simulations of Film Cooling Performance in the Showerhead Region of a Turbine Vane Including Conjugate Effects, ASME Paper No. IMECE2012-88386.

[20] Barigozzi, G., and Ravelli, S., 2015, Combined Experimental and Numerical Study of Showerhead Film Cooling in a Linear Nozzle Vane Cascade, ASME Paper No. GT2015-42397.

[21] Rozati, A., and Tafti, D. K., 2008, Large-Eddy Simulations of Leading Edge Film Cooling: Analysis of Flow Structures, Effectiveness and Heat Transfer, Int. J. Heat Fluid Flow, 29(1), pp. 1–17.

[22] Rozati, A., and Tafti, D. K., 2008, Effect of Coolant-Mainstream Blowing Ratio on Leading Edge Film Cooling Flow and Heat Transfer—LES Investigation, Int. J. Heat Fluid Flow, 29(4), pp. 857–873.

[23] Takahashi, T., Funazaki, K., Salleh, H. B., Sakai, E., and Watanabe, K., 2011, Assessment of URANS and DES for Predictions of Leading Edge Film Cooling, J. Turbomach., 134(3), p. 031008.

[24] Ravelli S., Barigozzi G., 2017, Comparison of RANS and Detached Eddy Simulation Modeling Against Measurements of Leading Edge Film Cooling on a First-Stage Vane. J. Turbomach., 139, 051005.

[25] ISSI, 2015, Binary FIB Pressure Sensitive Paint, Innovative Scientific Solutions, Inc., Dayton, OH, http://www.psp-tsp.com/

[26] Jahanmiri M. (2011) Pressure Sensitive Paints: The Basic and Applications. Research Report 2011:07; Chalmers University of Technology, Goteborg, Sweden.

[27] Han J-C, Rallabandi AP (2010) Turbine Blade Film Cooling Using PSP Technique. Frontiers in Heat and Mass Transfer. 1:013001. doi:10.5098/hmt.v1.1.3001.

[28] Natsui G et al., 2016, A Detailed Uncertainty Analysis of Adiabatic Film Cooling Effectiveness Measurements Using Pressure-Sensitive Paint, J. Turbomach., 138(8), 081007.

[29] Abdeh, H., Miranda M., Rouina S., Barigozzi, G., 2017, Development of PSP technique for Vane Film Cooling Investigations, Energy Procedia, 126, 802-809.

[30] Armellini A., Casarsa L., Mucignat C., 2011, Flow Field Analysis Inside a Gas Turbine Trailing Edge Cooling Channel Under Static and Rotating Conditions, Int. J. Heat and Fluid Flow, 32, pp. 1147-1159.

[31] Casarsa L. Giannattasio P., 2008, Three-Dimensional Features of the Turbulent Flow Through a Planar Sudden Expansion, Physics of Fluids, 20, 015103-1-15.

[32] Shiou-Jiuan, L., Shang-Feng, Y., and Je-Chin, H., Effect of Coolant Density on Leading Edge Showerhead Film Cooling Using PSP Measurement Technique," J. Turbomach., GT2013-94189, pp. V03BT13A005.

[33] Cutbirth, J. and Bogard, D., 2003, Effects of Coolant Density Ratio on Film Cooling, ASME paper GT2003-38582.

Nomenclature

A	cross-section area
a_0, a_1, a_2	calibration coefficients
BR	blowing ratio
c	oxygen concentration
C	vane chord
D	hole diameter
DR	density ratio
H	vane height
H_{12}	shape factor
I	momentum flux ratio/light intensity
L	hole length
m	mass flow rate
Ma	Mach number
MW	molecular weight
N	number of samples/direction normal to the wall
P	pressure
R	light intensity ratio
rms	fluctuating velocity components
s	curvilinear coordinate
S	vane pitch
T	temperature
Tu	turbulence intensity
U	free stream velocity
Vel	time averaged in plane velocity
Vort	vorticity
X,Y,Z	cascade coordinate system
Zc	confidence coefficient
δ	boundary layer thickness
Δt	image separation time
ε	statistical error

η	adiabatic effectiveness
ρ	density

Subscripts

1	inlet
2	exit
av	average
ax	axial direction
c	cooling flow
∞	free stream
fg	foreign gas
is	isentropic condition
n	normal to the wall
ref	reference
t	total
x	approach stream direction
y	cross-stream direction
z	spanwise direction